Doppler writing and linewidth control for scanning beam interference lithography

Juan C. Montoya,[a] Chih-Hao Chang, Ralf K. Heilmann, and Mark L. Schattenburg
Space Nanotechnology Laboratory, Massachusetts Institute of Technology, Cambridge, Massachusetts 02139

(Received 5 July 2005; accepted 25 September 2005; published 1 December 2005)

Scanning beam interference lithography (SBIL) is a technique which is used to create large-area periodic patterns with high phase accuracy. This is accomplished by combining interference lithography and an *X-Y* scanning stage. We previously reported parallel scan mode in which the stage scans in a direction parallel to the interference fringes. Here we present a method called Doppler scanning. In this mode, the stage is scanned perpendicular to the interference fringes. In order to obtain high-contrast latent gratings in the exposed photoresist, several parameters must be controlled. These parameters include vibration, fringe period error, time delay (for Doppler writing), dose, beam overlap, and polarization. In this article we present results of how the time delay, fringe period error, and exposure dose effect the contrast and linewidth of our latent grating images. Furthermore, SBIL has a unique ability to read gratings in a metrology mode configuration. This article also describes how Doppler metrology mode allows us to measure the time delay of our system. © *2005 American Vacuum Society.* [DOI: 10.1116/1.2127938]

I. INTRODUCTION

The goal of scanning beam interference lithography (SBIL) is to produce large-area periodic patterns at high speeds with subnanometer phase accuracy. Applications for these patterns include metrology, spectroscopy, nanophotonics, and nanomagnetics.[1] Traditional interference lithography suffers from poor phase fidelity for large gratings. For example, in order to expose a large substrate, traditional interference lithography must expand the beam. This is done by using an optical system which converts the wave front into an expanding spherical wave. The interference pattern of spherical waves leads to hyperbolic phase distortion.[2] Alternatively, large collimating lenses may be used to produce plane-like wave fronts. However, due to abberations and figure error present in large optics it is challenging to produce gratings without significant phase distortion.

Scanning beam interfence lithography addresses this issue by using small diameter beams which traverse large optical components. The SBIL system [see Fig. 1(a)] includes an *X-Y* air-bearing stage to which is attached a resist-covered substrate. A stationary interferometer attached to the optical bench and supported by the granite air-bearing block provides a grating "image" on the substrate. In order to expose large areas on the substrate, the stage is scanned using two different approaches as shown in Fig. 1. In both methods the interference fringes are held stationary with respect to the substrate using fringe locking electronics and acousto-optic modulators.[3] The first method [Fig. 1(b)] consists of a parallel scan, in which the stage scans along a direction parallel to the interference fringes. At the end of the scan, at a location outside of the substrate, the stage is stepped over by a distance of approximately half a beam diameter or less. This allows the new scan to overlap with the previous scan and produces a uniform dose profile.[4]

In this article we present results on the implementation of Doppler scanning. In Doppler scanning, the stage is scanned along a direction perpendicular to the interference fringes [Fig. 1(c)]. High contrast gratings require the fringe locking algorithm to synchronize the interference fringes to the stage motion perpendicular to the fringes. For example, consider an *X-Y* coordinate system which is defined by the reference frame of the granite block shown in Fig. 1(a). Assume the interference fringes are aligned parallel to the Y axis. If the stage moves perpendicular to the fringes (X direction), and the fringes are held stationary with respect to the granite, smearing of the fringes occurs on the exposed photoresist. On the other hand, if the interference fringes are phase locked with the X stage motion, the interference fringes move with the substrate along X and a high-contrast grating is produced in the photoresist.

Doppler scanning offers the immediate advantage in that one could write gratings in any direction. For certain periodic patterns, this technique could offer advantages in terms of speed and phase averaging. For example, consider a radially chirped grating. The contour of constant periods for this pattern are located along concentric circles of radius ρ. In order to write this pattern using a parallel scan, at each radius ρ the stage would need to take discrete steps along a circular trajectory. This step and scan approach would be much slower than a Doppler scan in which each radial grating is continously written. Moreover, the Doppler scan approach would allow for a continous amplitude-weighted phase average across the interfering beam diameter. The parallel scan approach, on the other hand, would only allow for a discrete phase average over the interfering beam diameter.

Implementing Doppler writing requires synchronous motion of the stage with interference fringes of our system. In

[a]Electronic mail: montoya@mit.edu

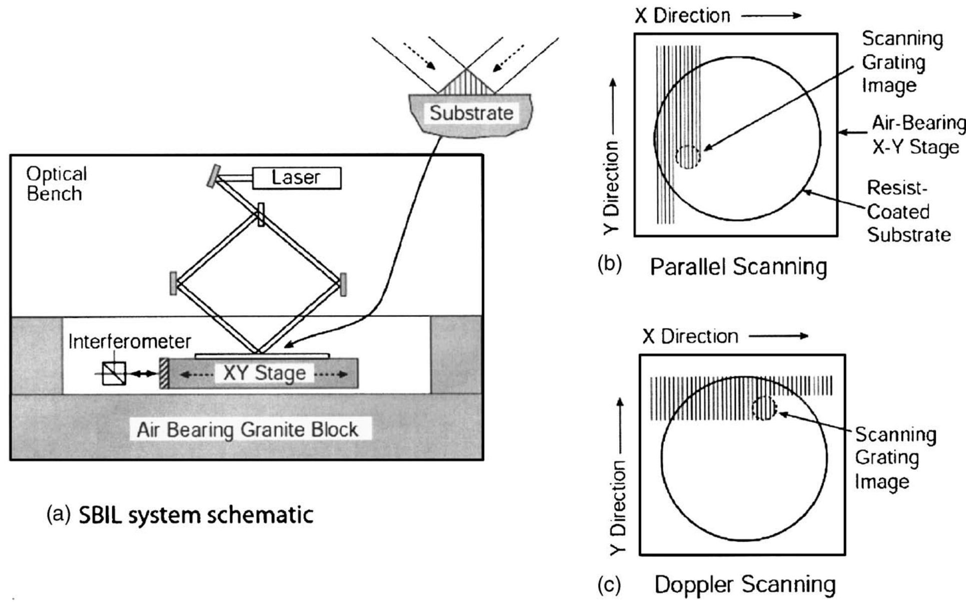

FIG. 1. (a) SBIL schematic showing X-Y stage and stage interferometer SBIL uses two scan methods to expose a large resist-covered substrate. In both methods, the interference fringes are held stationary with respect to the stage using phase-locking electronics. (b) Parallel scanning requires the stage to scan in a direction parallel to the interference fringes. The stage steps over less than half of the beam diameter off of the substrate at the end of a scan. A new strip is then written in the opposite direction which overlaps with the previous strip. (c) In Doppler scanning, the stage scans perpendicular to the interference fringes. The stage then steps over parallel to the interference fringes at the end of a scan.

order to accomplish this motion, high speed electronics are required. Here we will discuss the time delay associated with the time it takes to update the phase of the interference fringes from the time the stage position is acquired. Compensating for this time delay is necessary to implement Doppler writing. In this context, the time delay should not be confused with the temporal equivalent of an optical path length difference in the interfering arms.

II. DOPPLER WRITING

In order to implement Doppler writing our control loop uses five phase meter inputs. Two interfering arms using a $\lambda_{uv}=351.1$ nm wavelength produce a grating image on the substrate, as shown in Fig. 2. The left arm with frequency f_L is interfered with a heterodyne beam with frequency f_H in phase meter 1 (PM1), which outputs Φ_1. The right arm with frequency f_R is interfered with the heterodyne reference in phase meter 2 (PM2), which outputs Φ_2. The remaining three phase meters are necessary for stage control: the stage X-axis interferometer phase meter outputs the x stage position (Φ_x) in units of 2π phase corresponding to a distance $\lambda_{\mathrm{HeNe}}=632.8$ nm, the Y-axis interferometer outputs the y stage position (Φ_y) in the same phase units, and a refractometer phase meter which monitors variations in the index of refraction that lead to changes in optical path length. A detailed discussion of the refractometer phase meter is available elsewhere and is beyond the scope of this article.[5]

The difference between phase meter 1 and phase meter 2 in Fig. 2 obtains the phase difference $\Delta\Phi=\Phi_L-\Phi_R$ between the left and the right arms.[3] In order to implement Doppler writing, this phase must be synchronized with the stage motion. This requires significant frequency differences Δf between the arms, where $\Delta f=(1/2\pi)(d/dt)\Delta\Phi$. In order to describe the stage motion, we will define an X-Y reference frame to be that of the granite table on which the stage moves, as shown in Fig. 1.

For example, consider the case in which the image fringes formed by the left and right arms are parallel to the Y axis and periodic along the X axis with period $P_f=\lambda_{uv}/(2\sin\theta)$, where θ is the half-angle between the beams. The image intensity pattern will be of the form

$$I(x,t)=A\left\{1+\gamma\cos\left[\frac{2\pi}{P_f}x-\Delta\Phi(t)\right]\right\}G(x), \tag{1}$$

where A is the amplitude of the interference pattern, γ is the image contrast, x is the coordinate along the X axis, and $\Delta\Phi(t)$ is the phase difference of the left and right arms at time t. Here $G(x)=\exp[-8(x-x_0)^2/D^2]$ is the Gaussian envelope of the image, where x_0 is the image center and D is the e^{-2} diameter. During parallel scan mode $(d/dt)\Delta\Phi\approx 0$, leading to fringes essentially stationary with respect to the Gaussian envelope.

Now consider the reference frame of the moving stage. The stage reference frame X'-Y' is traveling at velocity $v(t)$ with respect to the stationary frame, which we assume is along the X axis. The moving stage coordinate relative to the stationary reference is therefore given by

$$x'=x-x_s, \tag{2}$$

where $x_s=\int v dt$. The intensity in the stage reference frame may then be written

$$I(x',t)=A\left\{1+\gamma\cos\left[\frac{2\pi}{P_f}(x'+x_s)-\Delta\Phi(t)\right]\right\}G(x'+x_s). \tag{3}$$

As the image envelope in the stage reference frame moves with time we want to frequency shift the left and right arms so that the fringes are stationary in the stage coordinate x'. We accomplish this by shifting the frequency of the two arms using acousto-optic modulators such that

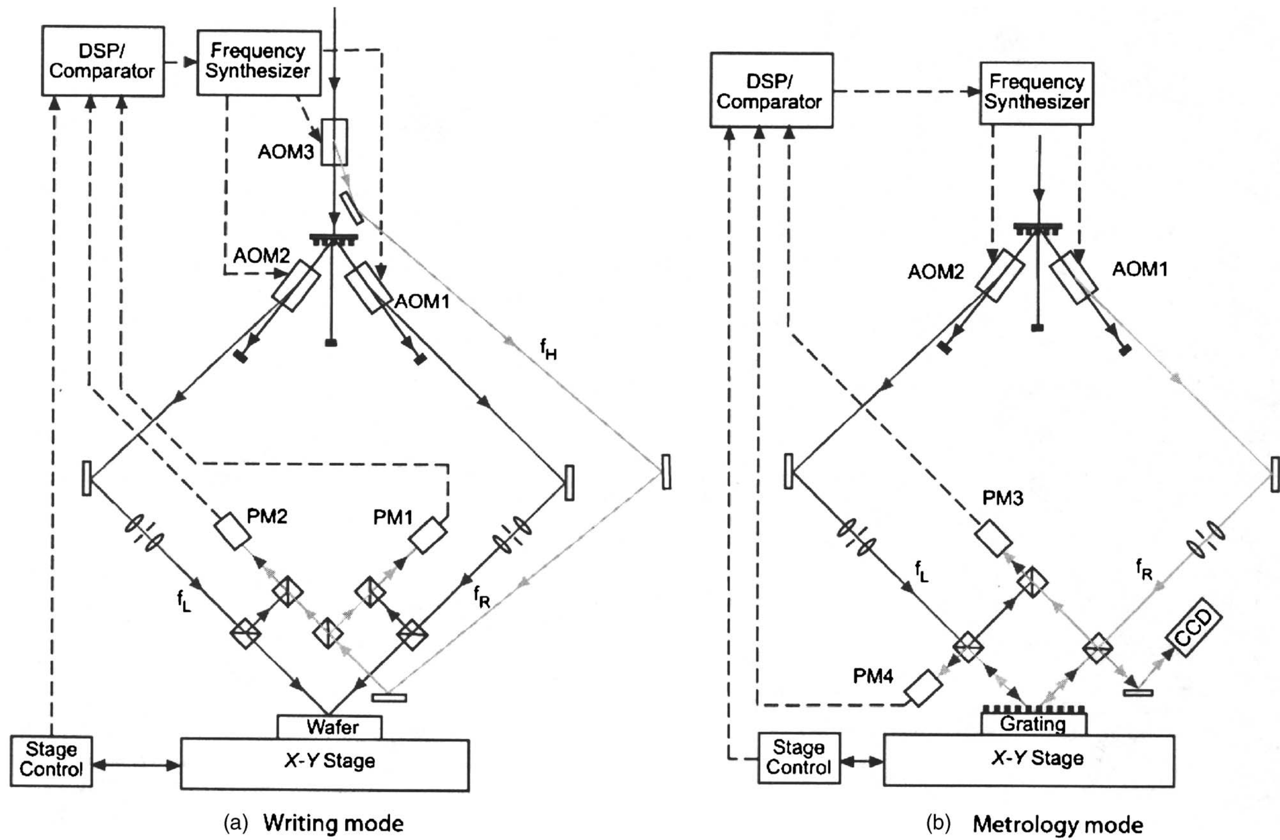

FIG. 2. Metrology and writing modes used in scanning beam interference lithography.

$$\frac{2\pi}{P_g}x_s = \Delta\Phi(t), \tag{4}$$

which can be written

$$\frac{2\pi}{P_g}\int v dt = 2\pi \int \Delta f dt, \tag{5}$$

where P_g is the desired grating period. For example, in the constant velocity case, $x_s = v \cdot t$ and the condition of fringe locking becomes $\Delta f = v/P_g$. In order to obtain high-contrast latent image in the resist, the difference between the fringe period and the grating period must be small otherwise fringe smearing will occur and contrast will degrade. This condition is met when $\Delta P/P_g \ll P_g/D$ where $\Delta P = P_f - P_g$ and D is the image diameter.

Early implementations of Doppler writing yielded gratings with poor contrast at certain velocities. This was determined to be due to the time delay in the control loop which results in phase offsets between overlapping scans. This is illustrated by including a time delay term t_d in Eq. (3), assuming constant velocity, obtaining

$$I(x',t) = A\left\{1 + \gamma \cos\left[\frac{2\pi}{P_f}(x' + x_s) - \frac{2\pi}{P_g}v \cdot (t - t_d)\right]\right\} \times G(x' + x_s). \tag{6}$$

The phase offset between adjacent scans is given by

$$\Phi_d = \frac{4\pi}{P_g}|v| \cdot t_d, \tag{7}$$

which increases with the velocity. In general, the above equation can be generalized to a two-dimensional case with the grating arbitrarily aligned with respect to the stage axes and with an arbitrary velocity vector. Note that at certain velocities where the phase offset $\Phi_d = (2n+1)\pi$, where n is an integer, the contrast in the printed image goes to zero and no grating results.

III. MEASURING THE TIME DELAY

We begin by identifying the various sources of time delay in our system. A set of five synchronized phase meters update internal phase registers at a 20 MHz clock rate (50 ns). Every 2000 cycles (100 μs) the phase meters simultaneously latch out their phase values making them available to externally readable registers, and generate a bus interrupt corresponding to a 10 kHz interrupt rate. A digital signal processor (DSP) services the interrupt at time T_i as shown in the timing diagram in Fig. 3.

The phases read by the DSP have a data age on the order of 335 ns as a result of time delays in electronics and digital filters.[6,7] In Fig. 3, the upper left inset shows the time T_i when the phase meters are latched and the interrupt routine begins. The phases which are latched at time T_i, however,

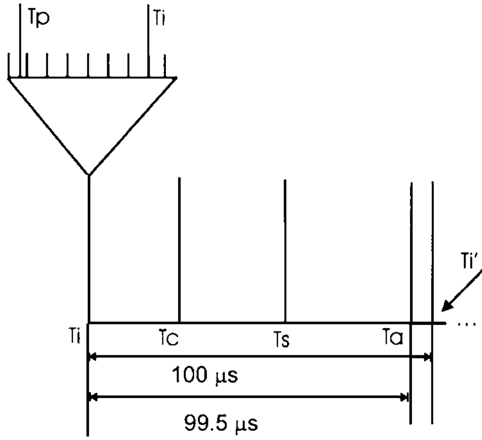

FIG. 3. Timing diagram of the SBIL control loop. Shown in the upper left is a zoomed-in view when the phase measurement occurs. At time T_i a DSP interrupt occurs. The phases which are available at T_i have a 335 ns delay time (T_i-T_p=335 ns) due to electronic propagation delay. The tick marks shown on the zoomed-in scale correspond to a period of the 20 MHz phase meter clock (50 ns). At time T_c, the DSP computes a phase correction and it is sent to the frequency synthesizer. At time T_s, the synthesizer outputs rf power to the AOM. At time T_a, the AOM frequency shifts the beam. The overall time delay T_a-T_p is 99.5 μs. At time $T_i'=T_i+100$ μs the next DSP interrupt occurs and the cycle repeats.

corresponds to the phase of the measurement signal at time T_p (335 ns delay). The comb in the inset corresponds to 50 ns events. Every 50 ns a new phase measurement occurs and the phases are summed and stored in internal phase registers.[6]

During the interval from T_i to T_c, the DSP reads the phase registers, calculates the phase error and outputs the phase correction to the digital frequency synthesizer (see Fig. 2). At time T_s the synthesizer outputs a radio frequency (rf) correction to the acousto-optic modulator (AOM). The propogation delay associated with the rf cable from the synthesizer to the AOM and the velocity of sound in the AOM transducer adds additional time. Finally, at time T_a the AOM phase shifts the beam and the beam propagates to the wafer. The overall time $t_d=T_a-T_p$ is the total time delay of the system measured to be 99.5 μs, which is just a little shorter than the DSP loop rate of 100 μs. Rather than determining the time delay of the various components individually, a series of experiments were used to determine the overall time delay of the system.

In order to measure the time delay of our control loop, a grating is mounted on the stage and the system is placed into metrology mode [see Fig. 2(b)]. In open-loop metrology mode SBIL uses two phase meters to measure the phase of gratings which have been previously written. Phase meter 4 measures the interference of the left arm backdiffracted off of the grating and the right arm zero-order reflected from the grating, obtaining

$$\Phi_4 = \Phi_L - \Phi_R - \Phi_g = \Delta\Phi - \Phi_g, \tag{8}$$

where Φ_L and Φ_R are the phase of the left and right arm, respectively, and Φ_g is the phase of the grating.[5,8]

Phase meter 3 measures the interference of the left and right arms which are picked off before they reach the grating, obtaining

$$\Phi_3 = \Delta\Phi = \Phi_L - \Phi_R. \tag{9}$$

Subtracting the output of phase meter 4 from phase meter 3 results in the phase of the grating Φ_g. The stage can be scanned in a parallel fashion, or in a Doppler scan mode. We developed a "closed-loop" Doppler configuration which allows measurement of the overall time delay of our feedback loop. In closed-loop Doppler metrology mode the stage is scanned perpendicular to the fringes, and a feedback loop synchronizes the phase of the image grating with the stage motion.

To illustrate this principle, lets confine ourselves to a one-dimensional example where the grating lines are periodic along the X axis of the stage. Furthermore, we scan the stage along the X axis. The phase of a constant-period grating in the stage frame is given by $\Phi_g=2\pi x'/P_g$. The phase of the grating in the stationary frame is given by

$$\Phi_g = \frac{2\pi}{P_g} \cdot (x - x_s), \tag{10}$$

where x_s is the grating position at time t in the stationary reference frame. In closed-loop Doppler metrology mode, the phase of the left and right arms are controlled such that the phase difference is given by

$$\Delta\Phi = 2\pi \frac{x_s}{P_m}, \tag{11}$$

where P_m is a constant to be determined. Taking the derivative of Eq. (11) yields

$$\Delta f = \frac{1}{2\pi}\frac{d}{dt}\Delta\Phi = v/P_m. \tag{12}$$

The output of phase meter 4 is given by $\Phi_4(t)=\Delta\Phi(t-t_d)+\Phi_g$. Expanding in a Taylor series about t yields

$$\Phi_4(t) = \Delta\Phi(t) - \frac{d}{dt}\Delta\Phi \cdot t_d + \Phi_g = \frac{2\pi}{P_m}(x_s - vt_d) + \frac{2\pi}{P_g} \times (x - x_s). \tag{13}$$

Note that the terms involving x_s cancel if the modulation constant $P_m=P_g$. Note also that the offset in phase depends on the product of the velocity and the time delay t_d.

Figure 4 shows the results of our closed-loop Doppler metrology mode experiment. The output of phase meter 4, Φ_4, is scaled by $P_m/2\pi$ to give units of microns. A hysteresis curve is obtained as the stage is scanned repeatedly back and forth, starting at rest at point A and accelerating in the positive direction to point B, then traveling with a velocity of +60 mm/s for ≈60 mm to point C corresponding to the upper portion of the hysteresis curve, then decelerating from point C to point D at rest, then accelerating in the negative direction from point D to point E, then traveling with a velocity of −60 mm/s for ≈60 mm to point F corresponding to the lower portion of the hysteresis curve, then finally decel-

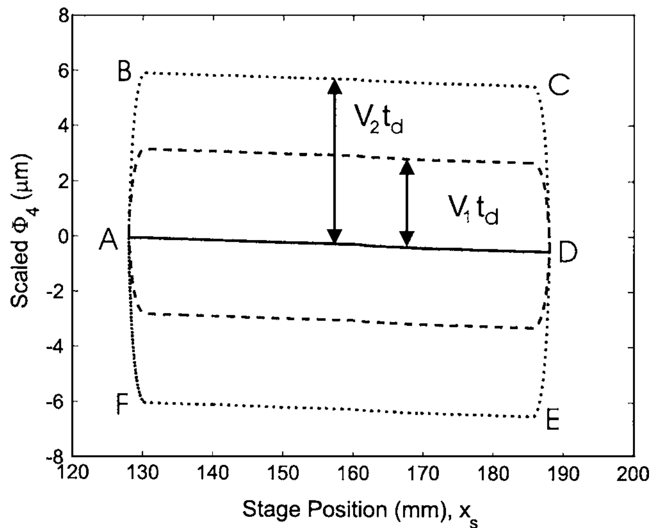

FIG. 4. Measured hysteresis curve of the Doppler metrology mode experiment used to determine the time delay. The upper portion of the curve (dotted line from *B-C*) corresponds to a positive stage velocity of v_2 =60 mm/s for 60 mm. The bottom portion (dotted line from *E-F*) corresponds to a negative velocity of 60 mm/s as the stage reverses its scan direction. Similarly, the dashed line corresponds to a velocity v_1 =30 mm/s. The offset from the center is proportional to the product of the velocity and time delay. Once the time delay is corrected for, the solid line in the center results in which the hysteresis is removed.

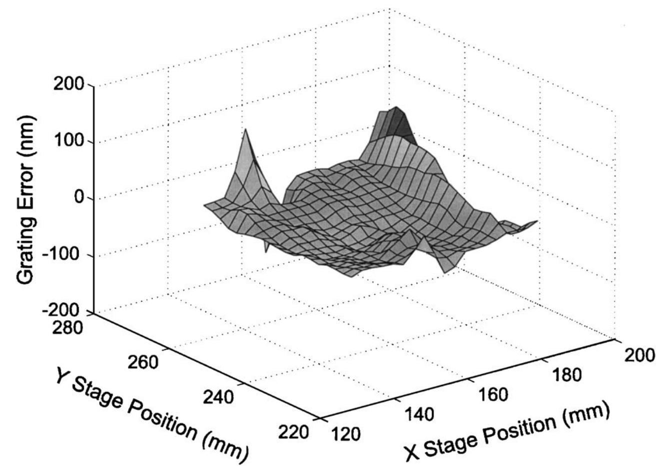

FIG. 5. Grating read in closed-loop Doppler metrology mode. Shown is a plot of the grating error in nanometers, after subtracting out a best-fit plane to the data.

erating to rest at starting point *A*. The offset from the center corresponds to the scaled phase delay, $\Phi_d \cdot P_g/2\pi = vt_d$, in units of length. This phase delay is proportional to the velocity of the stage and the time delay. Once the time delay is corrected for in the control loop, the hysteresis disappears and one obtains the dashed line in the center of the hysteresis loop shown in the figure. Ideally, the line should contain a zero slope. The slope in the line is a consequence of not matching the modulated constant P_m to the grating period P_g, resulting in a moiré beat between the two periods.

In order to further test Doppler metrology mode, a patterned grating is scanned using the closed-loop Doppler metrology mode and compared with the results of open loop metrology mode. The results obtained looked similar. Illustrated in Fig. 5 is a grating read in closed-loop Doppler metrology mode.

IV. LINEWIDTH CONTROL

There are various sources of contrast degradation which affect linewidth in SBIL. For Doppler writing, correcting for the phase offset due to time delay in the feedback loop is critical in order to obtain good contrast. Doppler writing in SBIL involves writing a strip perpendicular to the interference fringes and then stepping over by a fraction of the strip width (beam diameter) at the end of the scan [see Fig. 1(c)]. Subsequently, the scan direction is reversed and the next grating strip overlaps with the previous strip. This allows for building a uniform dose profile in the resist. As shown in the previous section, synchronization between the interference fringes and the stage motion is critical. A time delay in the electronics results in a phase offset between the positive and negative velocity scans. Figure 6 shows a plot of measured resist duty cycle (linewidth/period) for 574.303 nm period gratings with various time delays. The time delay of 99.5 μs results in the maximum linewidth for a given dose. The linewidths were measured using a scanning electron microscope. This further validates the Doppler metrology mode experiments, in which we measured the time delay of our system to be 99.5 μs.

There are several other sources of contrast degradation in SBIL. Some of these sources include beam overlap error, polarization error, vibrations, and fringe period error. Beam overlap error occurs when the two interfering beams which form the grating image have poor overlap. In the regions where the beams do not overlap, there is an absence of interference fringes and a background exposure results. As the resist-covered substrate is scanned, this region of blank exposure raises the average dose and lowers the contrast.

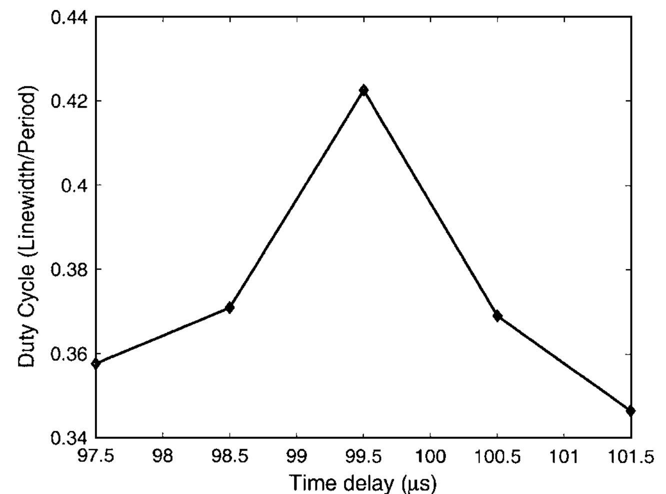

FIG. 6. Measured resist duty cycle (linewidth/period) for various time delays. The time delay corresponding to 99.5 μs results in the maximum contrast for a given dose. This measurement confirms the Doppler metrology mode experiments in which a 99.5 μs time delay was measured.

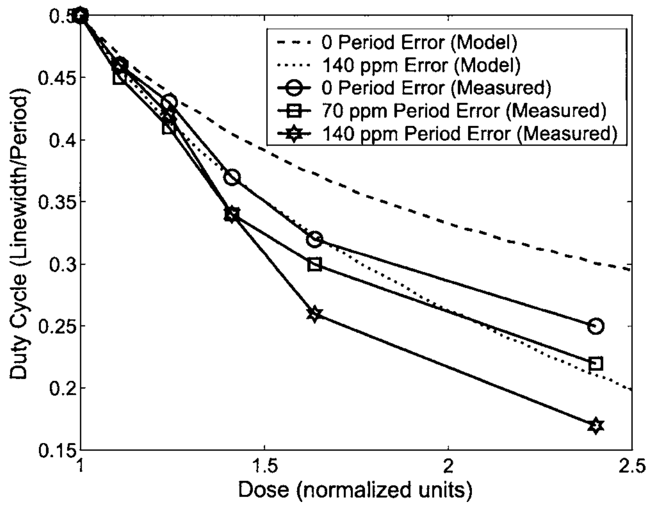

FIG. 7. Measured resist duty cycle (linewidth/period) vs dose for different period errors for 574.303 nm period gratings. The dashed and dotted lines show the result of a simulation where a period error of 0 and 140 parts per million are used. The solid lines indicate the results of measurement for a 0, 70, and 140 ppm period error. All plots intersect at the clearing dose, where the duty cycle is 50%.

Here we report on the contrast degradation due to fringe period error. In the case of parallel scanning, the fringes are held stationary and the stage is scanned in a direction parallel to the interference fringes. At the end of the scan the stage is stepped over by an integer number of fringe periods [see Fig. 1(b)]. This is necessary so that the peaks and valleys of the scan align with the peaks and valleys of the previous scan, thereby preserving contrast. A fringe period error will therefore lead to an incorrect step-over distance. The fractional period error is obtained from $\Delta P/P_g=(P_f-P_g)/P_g$, where P_f is the period of the fringes and P_g is the period of the grating being written.

A simulation for a Gaussian beam with a 1 mm radius, a step-over distance of 0.4285 mm, and a fringe period of 574.303 nm results in a contrast reduction of 7% for a 70 ppm period error. A 140 ppm period error is found to degrade the contrast by 25%. Figure 7 shows the results of a simulation for 0 and 140 ppm period error. This simulation assumes a binary resist model in which dose levels greater than the clearing dose of the resist are clipped (removed after developing), and an exposure dose below the clearing dose remains. The measured results for 574.303 nm period gratings are also shown in Fig. 7 for 0, 70, and 140 ppm period error. In these experiments, the dose is varied by changing the velocity of the stage. In effect, the velocity changes the exposure time of the beam on the resist. The formula which provides the average dose as a function of the velocity is given in units of $\mathrm{mJ/cm^2}$ by

$$\mathrm{Dose}=\frac{100P}{\Delta_{\mathrm{step}}v}, \tag{14}$$

where P is the total power in the interfering region given in milliwatts, v is the stage velocity in millimeters per second, and Δ_{step} is the step-over distance between scans in millimeters. An interesting feature shown in Fig. 7 is that all the curves intersect at the 50% duty cycle, which corresponds to the clearing dose. As the dose is increased for a given contrast, the linewidth shrinks as one would expect for positive resist. The slope of the linewidth versus dose curve gives an indication of the dose contrast. For high contrast, it is possible to overexpose beyond the clearing dose with less sensitivity to dose. For poor contrast, a more rapid decrease in linewidth is observed for overexposing beyond the clearing dose. For these experiments, wafers coated with 78-nm-thick Brewer i-con-4 ARC, and 570-nm-thick Sumitomo PFI-88 resist were used.

The experimental results and simulations show the trend one would expect. There is some discrepency, however, and the measured linewidths do not overlap with the simulations. One explanation for this involves using an oversimplified resist model. For this simulation, a binary resist model is used. Improved simulations would involve modeling higher-order effects in the resist, such as absorption, backreflections, and resist chemistry. In addition, other sources of contrast degradation may be present which are not being accounted for.

ACKNOWLEDGMENTS

The authors gratefully acknowledge the assistance of Robert Fleming of the MIT Space Nanotechnology Laboratory and support from NASA Grant Nos. NAG5-12583 and NAG5-5405.

[1] R. K. Heilmann, C. G. Chen, P. T. Konkola, and M. L. Schattenburg, Nanotechnology **15**, 2342 (2004).
[2] J. Ferrera, M. L. Schattenburg, and H. I. Smith, J. Vac. Sci. Technol. B **14**, 4009 (1996).
[3] R. K. Heilmann, P. T. Konkola, C. G. Chen, G. S. Pati, and M. L. Schattenburg, J. Vac. Sci. Technol. B **19**, 2342 (2001).
[4] C. G. Chen, P. T. Konkola, R. K. Heilmann, G. S. Pati, and M. L. Schattenburg, J. Vac. Sci. Technol. B **19**, 2335 (2001).
[5] P. T. Konkola, Ph.D. thesis, Department of Mechanical Engineering, Massachusetts Institute of Technology, Cambridge, MA, 2003.
[6] Zygo 2002 Measurement Board Manual OMP-0413F, Zygo Corp., Middlefield, CT.
[7] F. Demarest, Meas. Sci. Technol. **9**, 1024 (1998).
[8] P. T. Konkola, C. G. Chen, R. K. Heilmann, C. Joo, J. C. Montoya, C.-H. Chang, and M. L. Schattenburg, J. Vac. Sci. Technol. B **21**, 3097 (2003).